Stimulated thermal scattering induced by two-photon absorption and experimental observation of genuine stimulated Brillouin scattering in the near-ultraviolet region

V. B. Karpov* and V. V. Korobkin†

Coherent and Nonlinear Optics Department, A. M. Prokhorov General Physics Institute, Russian Academy of Sciences, Vavilov Street 38, 119991 Moscow, Russia

(Received 26 January 2007; published 10 June 2008)

Some of the experimental measurements of the frequency shift and phase conjugation fidelity gained from previous studies of stimulated scattering (SS) of nanosecond (5–10 ns) near-ultraviolet (uv) ($\lambda=193-351$ nm) laser pulses in liquids (hexane, heptane, and others) are found to disagree with the theory of SS, which takes into account only linear (single-photon) light absorption. To resolve the inconsistency, SS of XeCl excimer laser radiation ($\lambda=308$ nm) with the duration of 8 ns in liquid hexane is investigated experimentally. A theoretical analysis of the results obtained revealed three nonlinear optical phenomena induced by the heating due to two-photon absorption: stimulated thermal scattering (two-photon STS-2), phase mismatch for stimulated Brillouin scattering (SBS), and phase self-modulation. The experimental SS spectrum contains two additional lines—a two-photon STS-2 line and a genuine SBS line in the near-uv region.

DOI: 10.1103/PhysRevA.77.063812 PACS number(s): 42.65.Es, 42.65.Hw, 78.35.+c, 33.80.Rv

I. INTRODUCTION

Stimulated scattering (SS) is widely used in scientific research and practical applications [1–5]. This motivates studies of the physical mechanisms responsible for SS in various spectral regions. An important application is phase conjugation (PC) via stimulated backscattering [6]. Various SS mechanisms have specific characteristics (frequency shift, decay time, etc.) that manifest themselves in the PC mirror properties [4].

Detailed experimental studies of SS have been conducted only in the near-infrared (near-ir) region. For such experiments the pump radiation must have both high power and narrow bandwidth. The first sources of this kind were Q-switched single-mode ruby ($\lambda=0.69$ μm) and Nd:glass ($\lambda=1.06$ μm) lasers. For weak linear absorption, stimulated Brillouin scattering (SBS) and stimulated Raman scattering (SRS) were usually observed, and for stronger linear absorption stimulated thermal scattering caused by the heating due to linear absorption (linear STS-2).

In the first experimental studies of SBS with near-ir pump radiation [7–10], the unshifted spectral components were expected to be the pump spectral lines. But under the experimental conditions of [7–10], the pump spectral lines could not be distinguished from slightly shifted components corresponding, for instance, to linear STS-2. Multiphoton absorption could not influence the experiments because 5–10 near-ir photons with energies 1–2 eV would be required to obtain the nearest electron resonance with an energy about 10 eV.

Theoretical studies of SS have mostly relied on experimental results obtained for the near-ir region, and the modern SS theory applies only to linearly absorbing media [1–5,11,12]. The theory of stimulated thermal scattering (STS) proposed in [13,14] incorporates linear absorption only.

Reliable near-ultraviolet (near-uv) radiation sources (discharge XeF, XeCl, KrF, and ArF excimer lasers) became available considerably later than the solid-state near-ir lasers. When experimentalists in the 1980s had to deal with the PC via SS driven by excimer laser beams [15–22], the SS theory developed for the near-ir was applied to the near-uv spectral region.

II. PREVIOUS STUDIES OF STIMULATED SCATTERING AND PHASE CONJUGATION IN THE NEAR-ULTRAVIOLET REGION

The first studies concerning PC via SS in liquids (hexane, heptane, and others) were reported in [15] (XeF, $\lambda=351$ nm), [18] (XeCl, $\lambda=308$ nm), [16,19] (KrF, $\lambda=248$ nm), and [17] (ArF, $\lambda=193$ nm). In the above and subsequent studies [20,21], the experimental SS spectrum comprised a single shifted line, which was attributed to SBS. Note that the frequency shift of the SBS line in [17–19] was comparable to the laser system spectral resolution.

The reflection coefficient of the Brillouin mirror measured in [19] gradually decreased with increasing pump intensity I_L from 25% at the threshold ($I_L^{\mathrm{thr}}\approx 10^{10}$ W/cm^2) to 10% at $I_L\approx 10^{11}$ W/cm^2. Note that in this experiment the decrease in the reflection coefficient was due to the decrease in PC fidelity for the Brillouin mirror. In [15,16,18,20] the PC fidelity for the Brillouin mirror was found to degrade with increasing linear absorption coefficient α of the nonlinear liquid.

In [22] the experimental SS spectrum obtained in hexane by using KrF laser radiation also comprised a single line, which was attributed to linear STS-2. The linear absorption coefficient varied from $\alpha=0.02$ to 0.1 cm^{-1} in the studies of SBS [15–21] and amounted to $\alpha=0.22$ cm^{-1} in the investigation of linear STS-2 [22].

In order to increase the pump intensities in [15–22], the amplified laser beams were focused by lenses with focal lengths $F=5-10$ cm. The focal caustics corresponded to the volumes of the nonlinear interaction, and their lengths (see

*karpov@kapella.gpi.ru
†korobkin@kapella.gpi.ru

TABLE I. Previous studies of the stimulated backscattering in hexane for the near-uv pump radiation generated by ArF (193 nm), KrF (248 nm), XeCl (308 nm), and XeF (351 nm) excimer lasers

Reference	Pump wavelength λ (nm)	Pump intensity I_L (W/cm^2)	Experimentally measured frequency shift in hexane Ω (cm^{-1})	Physical mechanism of SS suggested by authors of the reference
[17]	193	$\approx 10^{10}$	≈ 0.2	SBS
[16]	248	$>2\times 10^{10}$	≈ 0.1	SBS
[19]	248	$>10^{10}$	≈ 0.1	SBS
[18]	308	$>10^{11}$	<0.15	SBS
[21]	308	$>10^{12}$	0.24	SBS
[15]	351	$>5\times 10^{9}$	0.2	SBS
[22]	248	$>10^{11}$	<0.02	Linear STS-2

Sec. VI B) were $L \leq 0.1$ cm. A considerable intensity attenuation due to the linear absorption over such distances occurs when $\alpha > 1$ cm^{-1}, which exceeds the values mentioned above. The pump pulse durations in [15–22] were $\tau_0 = 5-10$ ns.

Table I summarizes the results gained from the previous studies of stimulated backscattering in hexane for near-uv pump radiation. The first column presents a reference to the previous study; the second and third columns the pump wavelength λ and intensity I_L; the fourth column is the experimentally measured frequency shift Ω; and the last column is the physical mechanism that the authors of the reference believed to be responsible for the observed SS.

III. INCONSISTENCY BETWEEN PREVIOUS EXPERIMENTAL RESULTS AND THE EXISTING THEORY OF STIMULATED SCATTERING

A. SBS frequency shift

No one in the previous studies of SBS [15–21] calculated the theoretically predicted frequency shift to compare it with the experimentally measured one. In accordance with the existing theory [1–5], the SBS frequency shift Ω_B depends on the pump frequency ω_L (the pump wavelength λ) and the scattering angle θ [see Eq. (13) below]. Table II shows the values of Ω_B calculated for hexane, $\theta = \pi$, and the pump wavelengths listed in Table I (for the material data see Sec. VI C). It is clear that for the same λ the predicted values (Table II) disagree with the measured values attributed to SBS (Table I). The disagreement, which is too large to be entirely caused by experimental errors, emerges for pump wavelengths ranging from $\lambda = 193$ to 351 nm.

TABLE II. Theoretically predicted backward ($\theta = \pi$) SBS frequency shift Ω_B in hexane for the pump wavelengths listed in Table I.

Pump wavelength λ (nm)	Theoretically predicted SBS frequency shift in hexane Ω_B (cm^{-1})
193	0.49
248	0.41
308	0.33
351	0.30

B. Phase conjugation fidelity for Brillouin mirror

The decrease in PC fidelity for increased pump intensity above its threshold value detected in [19] is not dependent on SBS, because, in accordance with existing theory [4,11], strong pump saturation improves the discrimination of noise sources.

C. Emergence of linear STS-2 component and disappearance of SBS component

Emergence of the linear STS-2 component in [22] was explained by the increase in the linear absorption coefficient from $\alpha = 0.02-0.1$ cm^{-1} mentioned in [15–21], to $\alpha = 0.22$ cm^{-1}. But it was not explained how such an increase in α could cause the suppression of SBS in [22]. Indeed, the SBS component has been observed in [15–21] for practically the same experimental conditions as in this paper.

IV. EXPERIMENTAL SETUP

The problem concerns the understanding of both the temporal and the spatial behavior of the back-reflected pulses manifested in the frequency shift and the PC fidelity, respectively. The abnormal SBS was detected in a variety of studies conducted by a number of laboratories for nearly a decade [15–21], which rules out accidental experimental errors. This problem may be resolved by examining the fundamental physical mechanisms responsible for SS.

To investigate the physical mechanisms responsible for stimulated backscattering of nanosecond near-uv pulses, we constructed the experimental setup (Fig. 1) based on two commercially available ELI-91 XeCl excimer lasers ($\lambda = 308$ nm). The setup was designed as a master-oscillator–power-amplifier (MOPA) system. Hexane was used as the nonlinear liquid.

A. Master Oscillator

The master oscillator generates a weak narrow-bandwidth beam, whose diffraction-limited divergence was created by

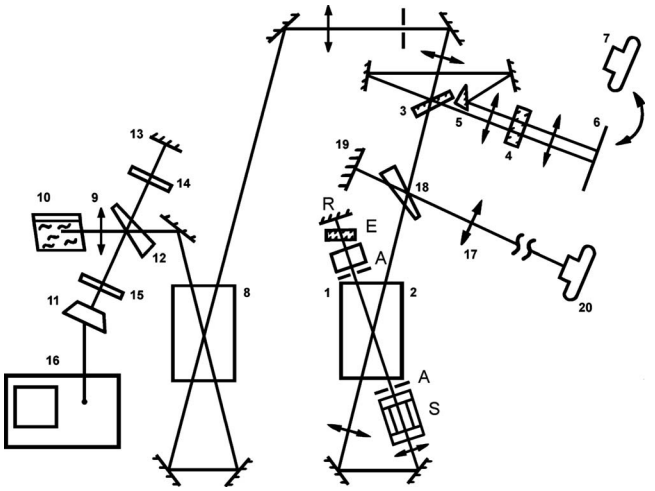

FIG. 1. Experimental setup for the investigation of the stimulated backscattering of a XeCl excimer laser beam in hexane: (1) the master oscillator and (2) the preamplifier based on the first ELI-91 XeCl laser; (3), (12), and (18) beam splitters; (4) the Fabry-Pérot étalon and (5) the prism of the spectrum analyzer; (6) the luminescent screen; (7) and (20) cameras; (8) the two-pass amplifier based on the second ELI-91 XeCl laser; (9) the lens with one of three possible focal lengths $F=11$, or 50, or 100 cm; (10) the cell filled with hexane; (11) the FEK-29KPU photodiode and (16) the S7-19 oscilloscope of the time-domain analyzer; (13) and (19) back-reflecting mirrors; (14) and (15) the neutral filters; (17) the divergence analyzing lens with the focal length $f_1=3$ m.

two apertures A of radius $r_0=0.8$ mm mounted one on each side of the MO active cell. The bandwidth was narrowed by means of a cavity consisting of a nontransparent mirror R at one end and a mode selector S at the other. The selector operates as an interference filter with a frequency-dependent reflection coefficient. Originally [23], a selector of this kind was used in a Nd:glass laser characterized by a spontaneous lifetime close to 1 μs. The spontaneous lifetime for a XeCl laser is about 20 ns. For a 1-m-long cavity, this yields six round trips, which is not sufficient to select a single longitudinal mode. The optical system proposed in [23] is useless when applied to the XeCl laser. However, a single longitudinal mode was selected by using an extra Fabry-Pérot étalon E placed inside the MO cavity. The MO output characteristics are presented in the third column of Table III; the characteristics of a commercially available ELI-91 laser are listed in the second column.

B. Experimental technique

The beam generated by MO 1 was expanded by a telescope and preamplified in the same active volume 2 of the first ELI-91 XeCl laser to approximately 1 mJ. After going twice through the amplifier 8 using the second ELI-91 XeCl laser head, the pulse achieved a nearly Gaussian temporal shape of 8 ns duration [full width at half maximum (FWHM)], 3 mJ energy, and 5×10^{-3} cm^{-1} bandwidth. Characteristics of the amplified beam are specified in the last column of Table III.

The amplified beam was focused by lens 9 into cell 10, filled with hexane. The nonlinear interaction took place in the focal caustic of lens 9. The backscattered wave traveled back through the system and was amplified in 8.

Beam splitter 12 was used to guide both forward- and backward-propagating beams into the time-domain analyzer. The temporal power profiles were measured by means of the FEK-29KPU photodiode 11 (the resolution being equal to 200 ps) and S7-19 oscilloscope 16 (the bandwidth being equal to 5 GHz). The phase-conjugation mirror reflectivity was determined as the ratio of the backscattered beam to the amplified beam peak power.

Beam splitter 3 was used to guide both forward- and backward-propagating beams into the spectrum analyzer (Fabry-Pérot étalon 4 with a variable dispersion-free region combined with prism 5), which produced the composite temporal spectrum of both the pump wave and the stimulated backscattered wave simultaneously on luminescent screen 6 or camera 7. This facilitated the measurement of the relative frequency shift. The temporal spectra were not changed by amplification in 8.

Beam splitter 18 was used to guide both forward- and backward-propagating beams into the divergence analyzer. For each beam, camera 20 created a photographic image of the focal spot produced by lens 17 with the focal length $f_1=3$ m. This photographic image carries only the amplitude information. Since the phase modulation gets transformed into an amplitude modulation in the focal region as in the far field, the beam divergence θ_L can be calculated from the relation $\theta_L\approx d/f_1$, where d is the focal spot diameter. In order to measure the amplified beam divergence the divergence analyzer was placed downstream of amplifier 8.

C. Nonlinear liquids and cells

In the previous experiments [15–22], the amplified beams were focused by lenses with the focal lengths $F=5-10$ cm

TABLE III. Laser parameters.

Parameter	Commercially available ELI-91 laser	Master oscillator	Amplified beam
Bandwidth (cm^{-1})	15	5×10^{-3}	5×10^{-3}
Aperture	10×20 mm^2	$\phi1.6$ mm	8×10 mm^2
Divergence (rad)	10^{-2}	6×10^{-4}	3×10^{-4}
Pulse duration (FWHM) (ns)	20	8	8
Pulse energy (mJ)	50	5×10^{-2}	3
Wavelength (nm)	308	308	308

into about 5-cm-long cells filled with nonlinear liquids. Organic solvents utilized in uv chromatography, such as hexane, heptane, and ethanol, were used as the nonlinear liquids. Similar results were obtained for different liquids. Since hexane (C_6H_{14}) was investigated in almost all of these studies (see Table I), we also chose it.

In our experiments, the amplified beam was focused by lens 9 into the center of cylindrical glass cell 10 with internal diameter 40 mm, filled with hexane. We used 5-cm-long cells in combination with lens 9 having $F=11$ cm and 30-cm-long cells in combination with lens 9 having $F=50$ and 100 cm. Each cell was sealed by two fused-silica input-output windows inclined at the angle of 5° to avoid parasitic reflections.

We used the high-performance liquid chromatography grade hexane produced by Oldrich Chemical Co., Milwaukee, WI, and chemically pure hexane from Russian suppliers. Their linear absorption coefficients measured at $\lambda=308$ nm were $\alpha=0.01\pm0.003$ and 0.046 ± 0.003 cm^{-1}, respectively. We added extremely small amounts of acetone to the hexane to slightly increase the linear absorption coefficient, so that the liquids used in our cells were characterized by $\alpha=0.01,0.046,0.08,0.17$ cm^{-1} at $\lambda=308$ nm.

The refractive index of hexane at $\lambda=308$ nm and its temperature derivative at constant pressure are [2] $n\approx1.4$, $(\partial n/\partial T)_p=-53\times10^{-5}$ K^{-1}. The corresponding permittivity and its derivative are $\varepsilon=n^2\approx2$,

$$\left(\frac{\partial\varepsilon}{\partial T}\right)_p=\frac{\partial\varepsilon}{\partial n}\left(\frac{\partial n}{\partial T}\right)_p=2n\left(\frac{\partial n}{\partial T}\right)_p\approx-1.5\times10^{-3}\ K^{-1}.$$

V. EXPERIMENTAL RESULTS

A. Experiment 1: The dependence of the temporal stimulated backscattering spectrum on the pump intensity

When constant parameters of the amplified beam (see Table III) are maintained, the pump intensity in cell 10 (see Fig. 1) can be varied by means of neutral filters or by changing the focal length of lens 9. The SS was close to its threshold for any lens 9 employed. Therefore, we could not use neutral filters, which reduce the amplified beam power. The pump intensity I_L was varied only by changing the focal length F of lens 9.

Three different lenses 9 with $F=11$, 50, and 100 cm were used. For each lens ($F=$const), the temporal spectrum was obtained by the spectrum analyzer described above with the Fabry-Pérot étalon 4 having a dispersion-free region of 0.66 cm^{-1}. Only the chromatography-grade hexane ($\alpha=0.01$ cm^{-1}) was used.

Figure 2 shows three images corresponding to the three values of F. Each photograph comprises two parts: the pump spectrum (right) and the stimulated backscattered spectrum (left). The stimulated backscattered spectrum has a single unshifted component when $F=11$ cm [Fig. 2(a)]; two components when $F=50$ cm, an unshifted one and a Stokes one shifted by 0.33 cm^{-1} [Fig. 2(b)]; and a single Stokes component shifted by 0.33 cm^{-1} when $F=100$ cm [Fig. 2(c)].

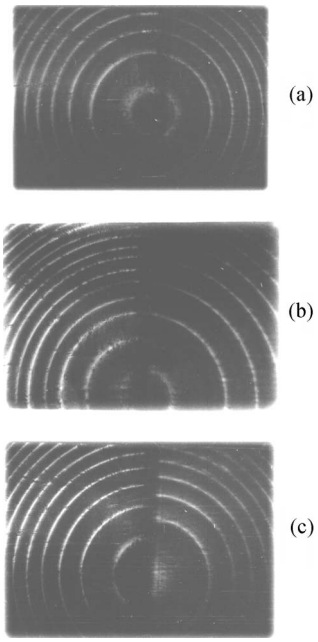

FIG. 2. Results of experiments 1 and 2: three temporal spectra obtained by the spectrum analyzer with Fabry-Pérot étalon 4 having the dispersion-free region of 0.66 cm^{-1}. Each photograph comprises two parts: the pump spectrum (right) and the stimulated backscattered spectrum (left) in hexane at a constant linear absorption coefficient α for three focal lengths of lens 9: $F=$ (a) 11, (b) 50, and (c)100 cm. The dependence of the stimulated backscattering spectrum on F is similar for $\alpha=0.01,0.046,0.08$ cm^{-1}.

B. Experiment 2: The dependence of the temporal stimulated backscattering spectrum on the linear absorption coefficient

We used all cells having $\alpha=0.01,0.046,0.08,0.17$ cm^{-1}. For each $\alpha=$const we examined the dependence of the stimulated backscattering spectrum on the pump intensity, which was controlled by changing the focal length of lens 9. The dependence on F for $\alpha=0.046,0.08$ cm^{-1} was similar to that for $\alpha=0.01$ cm^{-1} illustrated by Figs. 2(a)–2(c). Each stimulated backscattering spectrum obtained for $\alpha=0.17$ cm^{-1} contained a single unshifted component [as in Fig. 2(a)].

C. Experiment 3: The dependence of the phase-conjugation fidelity on the pump intensity

When the forward-propagating beam passes amplifier 8, its divergence increases by a factor of 3. We measured the divergences of forward- and backward-propagating beams at the location of beam splitter 18 with the help of the divergence analyzer described above. We examined the dependence of the backward-propagating beam divergence on the pump intensity, which was controlled by changing the focal length of lens 9. We used only the chromatography-grade hexane ($\alpha=0.01$ cm^{-1}) to avoid the thermal self-action caused by linear absorption. The experiment provided information on the phase-conjugation fidelity: when the PC fidelity is "high," the forward and backward aberrations must compensate each other.

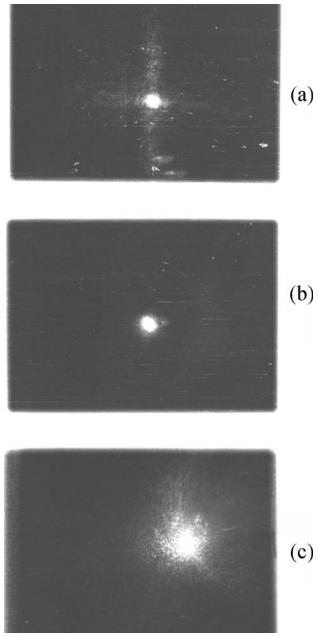

FIG. 3. Results of experiment 3: three focal spots obtained by the divergence analyzer for (a) the forward-propagating beam; (b) the backward-propagating beam ($F=100$ cm, high phase-conjugation fidelity); (c) the backward-propagating beam ($F=11$ cm, poor phase-conjugation fidelity). Images (b) and (c) were obtained for hexane with $\alpha=0.01$ cm^{-1}.

Figure 3 shows three photographic images created by camera 20. The resulting divergences are $\theta_L \approx 3\times10^{-4}$ rad for the forward-propagating beam [Fig. 3(a)]; $\theta_L \approx 3\times10^{-4}$ rad for the high phase-conjugation fidelity backscattered beam obtained with $F=100$ cm [Fig. 3(b)]; and $\theta_L \approx 2\times10^{-3}$ rad for the poor phase-conjugation fidelity backscattered beam obtained with $F=11$ cm [Fig. 3(c)].

D. Experiment 4: The temporal power profiles and the phase-conjugation mirror reflectivity

The analysis of the temporal evolution of the pulses with the time-domain analyzer described above is important, because the nonlinear mirror may change their amplitudes, durations, and shapes. All the liquids used had $\alpha=0.01, 0.046, 0.08, 0.17$ cm^{-1}.

The backscattered temporal power profile was found to have a nearly Gaussian shape and the duration (FWHM) of approximately 7 ns. The slightly shorter duration as compared to that of the pump (see Table III) can be attributed to the threshold nature of SS. The phase-conjugation mirror reflectivity reached 20% for $\alpha=0.01$ cm^{-1} and gradually decreased with increasing α. The reflectivity increased as the focal caustic of lens 9 was shifted from the center toward the input window of cell 10.

VI. ANALYSIS AND INTERPRETATION OF EXPERIMENTAL RESULTS

A. Results of experiments that require theoretical analysis

The observations in our experiments 1–4 on stimulated backscattering in hexane for different values of α and F that require further theoretical analysis can be summarized as follows.

(1) The dependence of the backscattering spectrum on F obtained for $\alpha=0.01-0.08$ cm^{-1} (a) the presence of two components when $F=50$ cm, an unshifted one (with the experimental error 0.02 cm^{-1}) and the Stokes one shifted by 0.33 cm^{-1} [Fig. 2(b)]; (b) the disappearance of the unshifted component when F is increased from 50 to 100 cm [Figs. 2(b) and 2(c)]; (c) the disappearance of the shifted component when F is reduced from 50 to 11 cm [Figs. 2(a) and 2(b)].

(2) The dependence of the backscattering spectrum when α is varied from 0.01 to 0.08 to 0.17 cm^{-1}: (a) the disappearance of the shifted component when $F=50$, 100 cm; (b) the appearance of the unshifted component when $F=100$ cm.

(3) The substantial decrease in the phase-conjugation fidelity obtained when at $\alpha=0.01$ cm^{-1} F is reduced from 100 to 11 cm [Figs. 3(b) and 3(c)].

B. Specific features of the stimulated scattering in our experiments

At the initial stage of the SS process, a weak scattered wave is generated as a result of the spontaneous scattering of the pump wave. In the resulting steady state without considerable pump saturation, the scattered wave intensity I_S is expressed as [1–5]

$$I_S(L) = I_S(0)\exp(I_L G L), \tag{1}$$

where $I_S(0)$ is the spontaneously scattered intensity, I_L is the pump intensity, G is the gain factor, and L is the nonlinear interaction length. The threshold condition for SS is

$$(I_L G L)^{\text{thr}} \approx 30. \tag{2}$$

If the total gain $(I_L G L)$ for a certain SS mechanism is below the threshold (2), the mechanism does not contribute to the overall SS pattern observed in an experiment.

Unfortunately, three-dimensional (3D) calculations of the real beam focal caustic are problematic even for vacuum. For organic liquids, only rough approximations can be used. Fortunately, in contrast to the near-ir, for the near-uv due to the fluorescence of hexane a blue track of the focused laser beam was simply observed through a thin transparent glass wall of the cell (of course, in a dark laboratory). The focal caustic geometry was measured and successively compared with the values calculated below.

The length of a light pulse with duration 8 ns is $L_P \approx 2.4$ m. The amplified beam with duration $\tau_0 \approx 8$ ns, divergence $\theta_L \approx 3\times10^{-4}$ rad, and radius $R_L \approx 0.5$ cm (Table III) was focused by lens 9. In accordance with Eq. (5), the length L of the focal caustic varied from $L_{\min} \approx 0.6$ mm for $F=11$ cm to $L_{\text{mid}} \approx 1.5$ cm for $F=50$ cm and $L_{\max} \approx 6$ cm for $F=100$ cm. The long-pulse condition $L_P \gg L$ is met for the entire range of values of F. At any moment of time, the pump power W_L can be treated as constant over the caustic length L, which is approximately equal to the length of the area where the nonlinear interaction occurs. To simplify the analysis, we assume that the pump intensity I_L is uniformly

distributed over a cylindrical focal caustic of diameter d_f and length L.

It should be noted that such a technique is frequently met in nonlinear optical studies. For instance, the impact of the focal caustic dimensions upon the optical breakdown threshold has been studied in [24]. Ruby laser pulses were focused by lenses of focal lengths $F=1-13$ cm into gases. The focal caustics were supposed to have cylindrical shapes, but their dimensions were not measured. The transition from the focal length to the focal spot diameter was performed with the help of the equation $d_f \approx F\theta_L$, where θ_L is the laser beam divergence. In contrast to [24], long-focal-length lenses with $F \geq 11$ cm were used in our experimental conditions. Moreover, due to the fluorescence of hexane, the focal caustics were seen with the naked eye, and for $F=50$ and 100 cm their lengths could be measured with a ruler.

When a laser beam with power W_L, radius R_L, and divergence θ_L is focused by a lens, the product $(I_L L)$ is independent of the focal length F of this lens. Indeed,

$$I_L \approx \frac{W_L}{S_f}, \tag{3}$$

$$S_f = \frac{\pi d_f^2}{4} \approx \frac{\pi (F\theta_L)^2}{4}, \tag{4}$$

$$L \approx \frac{d_f}{\theta_0/2} \approx \frac{F\theta_L}{R_L/F} = \frac{F^2\theta_L}{R_L}, \tag{5}$$

where W_L, R_L, θ_L are independent of F; $d_f \approx F\theta_L$; S_f is the cross-sectional area of the focal caustic; $\theta_0 \approx 2R_L/F$ is the convergence angle of the beam after the lens. We obtain

$$I_L \propto F^{-2}, \quad L \propto F^2 \Rightarrow (I_L L) \approx \text{const}. \tag{6}$$

The full expression is

$$(I_L L) \approx \frac{4W_L}{\pi\theta_L R_L} \approx \frac{4U_L}{\pi\theta_L R_L \tau_0}, \tag{7}$$

where U_L and τ_0 are the energy of the pulse and its duration, respectively. For the parameters of the amplified beam presented in Table III, Eq. (7) yields $(I_L L) \approx 3\times 10^3$ MW/cm. The amplified beam energy 3 mJ (Table III) corresponds to the absence of diagnostic equipment and reflects the maximum possible value for this laser system before cell 10. Due to the diagnostic and other energy losses between the exit of amplifier 2 and the focal caustic of lens 9, the real on-target energy is $U_L \approx 1.5$ mJ. Accordingly, we have $(I_L L) \approx 1.5 \times 10^3$ MW/cm.

There are two varying parameters in our experiments—α and F. As far as the variation of F is concerned, Eq. (6) shows that the value

$$(I_L L) \approx 1.5 \times 10^3 \text{ MW/cm} \tag{8}$$

is constant. Since $(I_L L) \approx$ const, the only parameter that may affect the left part of Eq. (2) via G is α. If the SS process does not involve heating due to linear absorption, G is independent of α, and the total gain $(I_L GL)$ does not change in our experiments.

The diameter of the amplified beam incident on lens 9 is $D_L \approx 1$ cm (Table III). The focal length of lens 9 is $F > 10$ cm. Therefore, $D_L/F < 0.1$, and the focal caustics were not distorted by spherical aberrations of lens 9 or by a jump in the refractive index across the air-cell boundary.

C. Parameters of SBS and linear STS-2 for our experimental conditions

Since SBS and linear STS-2 were considered responsible for the observed SS in the previous studies (see Table I), we should calculate their parameters for our experimental conditions.

1. Properties of SBS

According to the SBS model [1–5], the modulated electrostrictive force amplifies a hypersonic wave with wave vector $\mathbf{q}=\mathbf{k}_L-\mathbf{k}_S$ and frequency

$$\Omega_B = |\mathbf{q}|v, \tag{9}$$

where $\omega_L, \mathbf{k}_L$, and $\omega_S, \mathbf{k}_S$ denote the frequencies and the wave vectors of the pump and scattered waves; v is the speed of sound. The steady-state gain factor near the Stokes resonance peak is

$$G_B = \frac{\rho^2(\partial\varepsilon/\partial\rho)^2}{1+(\omega_L-\omega_S-\Omega_B)^2/\Gamma_B^2} \frac{\omega_S q^2}{4\Omega_B \Gamma_B \rho n^2 c^2}, \tag{10}$$

where ρ is the density, c is the speed of light, and n is the unperturbed refractive index. The decay rate Γ_B is related to the decay time τ_B:

$$\Gamma_B(\mathbf{q}) = A|\mathbf{q}|^2, \quad \tau_B \approx \Gamma_B^{-1}. \tag{11}$$

For liquids, $A=2\eta_1/3\rho$, where η_1 is the shear viscosity. The highest gain factor (10) is achieved when $\omega_L-\omega_S=\Omega_B$. When the scattered wave propagates at an angle θ relative to the pump wave,

$$q = |\mathbf{q}| = |\mathbf{k}_L - \mathbf{k}_S| \approx 2|\mathbf{k}_L|\sin(\theta/2) = 2(\omega_L n/c)\sin(\theta/2). \tag{12}$$

Accordingly, the SBS frequency shift is

$$\Omega_B = qv = 2\omega_L n(v/c)\sin(\theta/2). \tag{13}$$

2. Properties of linear STS-2

According to the linear STS-2 model [1–4,13], the modulated heating amplifies a thermal wave with wave vector $\mathbf{q}=\mathbf{k}_L-\mathbf{k}_S$. The steady-state gain factor is

$$G_T \approx \frac{\omega_S \alpha}{cn\rho c_p \Gamma_T} \left(\frac{\partial\varepsilon}{\partial T}\right) \frac{(\omega_L-\omega_S)/\Gamma_T}{1+(\omega_L-\omega_S)^2/\Gamma_T^2}, \tag{14}$$

where α is the linear absorption coefficient, c_p is the specific heat, and χ is the thermal diffusivity. The decay rate Γ_T is related to the decay time τ_T:

$$\Gamma_T = \chi|\mathbf{q}|^2, \quad \tau_T \approx \Gamma_T^{-1}. \tag{15}$$

Since $\partial\varepsilon/\partial T$ is negative for most substances, a positive gain corresponds to an anti-Stokes frequency shift $(\omega_L-\omega_S)<0$.

The highest gain factor (14) is achieved when $(\omega_L-\omega_S)=\Omega_T=-\Gamma_T$.

3. Predicted values of the SBS and linear STS-2 parameters for our experiments

Under our experimental conditions, the following numerical values [2,5,25] should be substituted into Eqs. (9)–(15):

$$\lambda = 308 \text{ nm}, \quad \theta = \pi, \quad \rho \approx 0.66 \frac{\text{g}}{\text{cm}^3}, \quad n \approx 1.4,$$

$$\eta_1 \approx 3.2 \times 10^{-3} P \approx 3.2 \times 10^{-3} \frac{\text{g}}{\text{cm s}},$$

$$v \approx 10^5 \frac{\text{cm}}{\text{s}}, \quad c \approx 3 \times 10^{10} \frac{\text{cm}}{\text{s}}, \quad \rho\left(\frac{\partial \varepsilon}{\partial \rho}\right)_T \approx 1,$$

$$\frac{\omega_S}{2\pi} \approx \frac{\omega_L}{2\pi} \approx 10^{15} \text{ Hz}, \quad \chi \approx 10^{-3} \frac{\text{cm}^2}{\text{s}},$$

$$\left(\frac{\partial n}{\partial T}\right)_P \approx -53 \times 10^{-5} \text{ K}^{-1},$$

$$\left(\frac{\partial \varepsilon}{\partial T}\right)_P \approx -1.5 \times 10^{-3} \text{ K}^{-1}, \quad c_P \approx 2.3 \frac{J}{\text{g K}},$$

$$\delta = \frac{c_P}{c_V} \approx 1.3.$$

The predicted SBS frequency shift is $\Omega_B=0.33$ cm^{-1} (see Table II). The hypersonic grating decay time is $\tau_B \approx 1$ ns. Since this time is shorter than the pump duration by a factor of 8, the steady-state model can be used. The frequency-optimized SBS gain factor (10) is expressed as

$$G_B = \frac{\omega_S q^2}{4\Omega_B \Gamma_B \rho n^2 c^2} = \frac{3}{16 n^3 c v \eta_1} \approx 0.07 \frac{\text{cm}}{\text{MW}}. \quad (16)$$

The predicted linear STS-2 frequency shift is $\Omega_T \approx -\Gamma_T \approx -0.01$ cm^{-1}. The thermal grating decay time is $\tau_T \approx 3$ ns. Even though it is shorter than the pump duration by almost a factor of 3, we cannot reliably use the steady-state model. Since we explore the possibility of the emergence of linear STS-2 in an experiment rather than attempting to maximize its efficiency, we do use the steady-state model to simplify the further analysis. The thermal-grating wavelength Λ_T associated with the backscattering is

$$\Lambda_T = \frac{2\pi}{q} \approx \frac{2\pi}{2k_L} = \frac{\lambda}{2n} \approx 10^{-7} \text{ m}. \quad (17)$$

The time of the pressure relaxation over Λ_T is

$$\tau_{\text{pr}} = \frac{\Lambda_T}{v} \approx 10^{-10} \text{ s}. \quad (18)$$

Since $\tau_{\text{pr}} \ll \tau_0$, G_T can be obtained by using the permittivity temperature derivative at constant pressure. The frequency-optimized linear STS-2 gain factor (14) is expressed as

$$G_T = \frac{\omega_S \alpha}{2cn\rho c_P \Gamma_T}\left(\frac{\partial \varepsilon}{\partial T}\right)_P = \frac{\alpha c}{8\omega_L n^3 \rho c_P \chi}\left(\frac{\partial \varepsilon}{\partial T}\right)_P \approx 0.2\alpha \frac{\text{cm}^2}{\text{MW}}. \quad (19)$$

TABLE IV. Gain factors G_T,G_B and total gains $(I_L G_T L)$,$(I_L G_B L)$ for linear STS-2 and SBS calculated for various values of α, but for constant $(I_L L) \approx 1.5 \times 10^3$ MW/cm (as in our experiments).

	Linear STS-2		SBS	
α (cm^{-1})	G_T (cm/MW)	$(I_L G_T L)$	G_B (cm/MW)	$(I_L G_B L)$
0.01	0.002	3	0.07	105
0.046	0.009	14	0.07	105
0.1	0.02	30	0.07	105

The frequency-optimized gain factors and total gains for linear STS-2 and SBS calculated for various values of α, but for constant $(I_L L) \approx 1.5 \times 10^3$ MW/cm, as in our experiments, are listed in Table IV. The first column of the table shows the linear absorption coefficient α; the second and fourth columns, the gain factors G_T and G_B; the third and the last columns, the total gains $(I_L G_T L)$ and $(I_L G_B L)$. The theoretical estimates presented in Table IV lead to the following conclusions.

Linear STS-2. The total gain (depending on α via G_T) is much lower than the threshold given by Eq. (2) both for the chemically pure ($\alpha=0.046$ cm^{-1}), and *a fortiori* for the chromatography-grade ($\alpha=0.01$ cm^{-1}) hexane. The threshold is reached when $\alpha=\alpha_{\text{STS}}^{\text{thr}} \approx 0.1$ cm^{-1}.

SBS. The total gain (independent of α) is higher than the threshold given by Eq. (2).

D. Emergence and disappearance of the spectral components in accordance with the existing theory

1. Shifted component of the stimulated backscattering spectrum

Since the total gain $(I_L G_B L)$ (Table IV) exceeds the threshold (2) and the measured value of the frequency shift 0.33 cm^{-1} [Figs. 2(b) and 2(c)] agrees with Eq. (13) (Table II), the shifted component should be attributed to SBS. To explain the absence of the shifted component in Fig. 2(a), we explore the possibility of SBS breakdown. The only mechanism that can suppress SBS under our conditions is phase mismatch [11,12]. When the permittivity of the medium changes with time due to the weak uniform heating caused by linear absorption with the coefficient α, the wavelengths of the pump and scattered waves vary. Since the acoustic wave has a finite response time, the phase matching conditions are violated. If $I_L(L)$ is the input pump intensity and $I_S(L)$ is the output backscattered intensity, then the SBS conversion efficiency over the length L of nonlinear interaction is $\eta=I_S(L)/I_L(L)$. The dependence of η on $I_L(L)$ is given by the relation [11,12]

$$h(D + \ln \eta) = \Gamma_B G_B \arctan[I_L(L)(1-\eta)Lh/\Gamma_B], \quad (20)$$

where $D \approx 30$, G_B is the peak backward SBS gain factor defined by Eq. (16), and

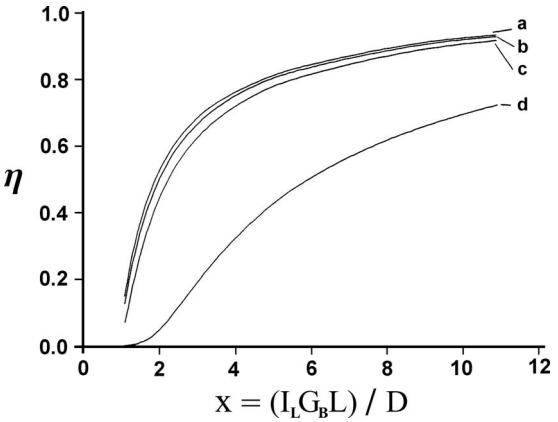

FIG. 4. Predicted SBS conversion efficiency η vs the total gain normalized to the threshold value $D \approx 30$ for hexane, for $\lambda = 308$ nm and $\alpha =$ (a) 0.0001, (b) 0.03, (c) 0.05, and (d) 0.1 cm^{-1}.

$$h = \frac{\alpha \omega_L}{2cn\rho c_p}\left(\frac{\partial \varepsilon}{\partial T}\right)_P.$$

Figure 4 shows the SBS conversion efficiency η as a function of the total gain normalized by its threshold value $x = (I_L G_B L)/D$, evaluated numerically by using the relation (20) for hexane, for $\lambda = 308$ nm, and for several values of α. The critical value corresponding to curve d is $\alpha_{cr} \approx 0.1$ cm^{-1}. For $\alpha = 0.01, 0.046, 0.08$ cm^{-1}, no SBS suppression due to phase mismatch should be expected.

2. Unshifted component of the stimulated backscattering spectrum

PC via SS can be caused by mechanisms other than SBS [1,3,4]. Since the measured frequency shift does not exceed 0.02 cm^{-1} (the experimental error), we should consider stimulated thermal scattering caused by heating due to the electrocaloric effect (STS-1), linear STS-2, and stimulated Rayleigh wing scattering (SRWS).

First, consider SRWS. Since the molecular anisotropy of liquid hexane is weak [26], the excitation of SRWS is impossible. Normally, the SRWS gain factor for liquids does not exceed $G_{RW} \approx 10^{-3}$ cm/MW [1]. For our condition (8) the SRWS total gain does not exceed $(I_L G_{RW} L) \approx 1.5$, which is much lower than the threshold (2).

Now consider STS-1. According to [1], the STS-1 to SBS gain factor ratio is

$$\frac{G_{RL}}{G_B} = \frac{(\delta - 1)c\Gamma_B}{4\pi v \omega_S}. \quad (21)$$

For our experimental conditions, $G_{RL}/G_B \leq 10^{-2}$. From the value of $(I_L G_B L)$ in the last column of Table IV, the STS-1 total gain is $(I_L G_{RL} L) \leq 1$, which is much lower than the threshold (2).

The processes of SRWS and STS-1 do not involve heating due to absorption of the radiation, and their total gains do not change in our experiments as long as $(I_L L)$ is constant (see Sec. VI B). The emergence of SRWS and STS-1 components under our experimental conditions is impossible.

Now consider linear STS-2. The predicted frequency shift $\Omega_T \approx -0.01$ cm^{-1} (see Sec. VI C 3) agrees with the measured one. Indeed, the absolute value of the latter is less than 0.02 cm^{-1} (the experimental error). Heating due to absorption of the radiation is involved in the linear STS-2 process, and its total gain varies with α while $(I_L L)$ is constant. The emergence of the linear STS-2 component under our experimental conditions (Table IV) is possible only when $\alpha \geq 0.1$ cm^{-1}.

E. Decrease in phase-conjugation fidelity in accordance with the existing theory

The only mechanism that can cause a decrease in the PC fidelity [Figs. 3(b) and 3(c)] under our experimental conditions is phase self-modulation [11,12]. Consider the following cylindrically symmetric problem in coordinates (R,z,t). A wave with a plane front and a spatially nonuniform intensity $I_L(R,t)$ enters a nonlinear medium at $t=0$ across a boundary located at $z=0$ and propagates toward a boundary located at $z=L$. The medium is characterized by the linear absorption coefficient α. Heat conduction does not contribute in the transverse coordinate R. The temperature increment over time t is

$$\delta T(R,t) = \frac{1}{\rho c_P}\int_0^t \alpha I_L(R,\tau)d\tau = \frac{\alpha}{\rho c_P}\int_0^t I_L(R,\tau)d\tau. \quad (22)$$

The refractive index depends on temperature, $n = n_0 + \delta n(T)$, where the nonlinear term is

$$\delta n(R,t) = \left(\frac{\partial n}{\partial T}\right)\delta T(R,t) = \left(\frac{\partial n}{\partial T}\right)\frac{\alpha}{\rho c_P}\int_0^t I_L(R,\tau)d\tau. \quad (23)$$

The wave vector is $\mathbf{k}(R,t) \approx \mathbf{e}_z k(R,t)$, where $k = k_0 + \delta k = (\omega/c)(n_0 + \delta n)$.

The nonlinear phase increment over the distance L is

$$\begin{aligned}\delta\Phi(R,t) = \delta kL &= \frac{\omega L}{c}\delta n(R,t) \\ &= \frac{\omega L}{c}\left(\frac{\partial n}{\partial T}\right)\frac{\alpha}{\rho c_P}\int_0^t I_L(R,\tau)d\tau \\ &= \frac{\omega}{c}\left(\frac{\partial n}{\partial T}\right)\frac{\alpha}{\rho c_P}\int_0^t I_L(R,\tau,F)L(F)d\tau. \quad (24)\end{aligned}$$

A wave with a plane front at $z=0$ will have a radially nonuniform front at $z=L$. The front distortion is zero at $t=0$ and maximal at the end of the pulse.

Due to the phase self-modulation of the pump wave, the backscattered wave gets coupled to the dynamically distorted beam. Taking into account the finite nonlinearity decay time, this effect may cause a decrease in PC fidelity.

It must be noted that lenses 9 as well as cells 10 (see Fig. 1) were changed only in the intervals between separate sets of experiments. The SS of a great number of pump pulses was studied in every set. That is why F is a parameter in the final form of expression (24), which remains invariant over the pump duration. For pump pulses from different sets of

experiments, at any instant τ the product $(I_L L)$ contained in (24) does not depend on F, as shown by Eq. (6). Therefore, $\delta\Phi(R,t)$ does not depend on F, and heating with α=const cannot explain the decrease in the PC fidelity when F is reduced from 100 to 11 cm.

Let us make numerical evaluations of $\delta\Phi$ for our experimental conditions:

$$\delta\Phi = \frac{\omega}{c}\left(\frac{\partial n}{\partial T}\right)\frac{\alpha}{\rho c_P}\int_0^t (I_L L)d\tau$$

$$\approx \frac{\omega}{c}\left(\frac{\partial n}{\partial T}\right)_P \frac{\alpha}{\rho c_P}(I_L L)\tau_0$$

$$\approx -\alpha\ (\mathrm{cm}^{-1}) \times 10^3\ \mathrm{rad}. \qquad (24')$$

For $\alpha=10^{-2}$ cm^{-1} we obtain $|\delta\Phi|\approx 10$ rad. Such a large value confirms the strong effect of the phase self-modulation. Equation (24) expresses the upper limit of the $\delta\Phi$ estimation. Indeed, first, the value of $(\partial n/\partial T)$ at constant pressure was used, but the pressure stabilization over the focal caustic requires time. Second, our model was developed for weak heating. For strong heating the heat conduction should be taken into account.

F. Implication of two-photon absorption in the theory of stimulated scattering

The existing SS theory developed for linearly absorbing media cannot explain our experimental results. First, since the linear absorption with $\alpha<0.1$ cm^{-1} is not sufficiently strong to give rise to linear STS-2, the physical mechanism responsible for the unshifted component observed for $\alpha=0.01-0.08$ cm^{-1} [Figs. 2(a) and 2(b)] remains unclear. Second, since the linear absorption with $\alpha<0.1$ cm^{-1} is not strong enough to suppress SBS via phase mismatch, the disappearance of the SBS component when F is reduced from 50 to 11 cm [Figs. 2(a) and 2(b)] observed for $\alpha=0.01-0.08$ cm^{-1} is yet to be explained. Third, the linear absorption with $\alpha=0.01$ cm^{-1}=const cannot explain the substantial decrease in the PC fidelity caused by the decrease in F from 100 to 11 cm [Figs. 3(b) and 3(c)].

Two-photon absorption should be expected in hexane for $\lambda<400$ nm [27]. Suppose that our experiments were strongly affected by the two-photon absorption. More specifically, assume that the unshifted component corresponds to the STS-2 process associated with the heating caused by two-photon absorption. We call this mechanism the two-photon STS-2, as distinct from the previously known mechanism induced by linear (single-photon) absorption, i.e., linear STS-2.

The intensity $I(z)$ of the radiation propagating along the z axis is governed by the following equation [1,28]:

$$\frac{dI}{dz} = -\gamma I^2, \qquad (25)$$

where γ is the two-photon absorption coefficient. Its solution is

$$I(z) = \frac{I_0}{1+I_0\gamma z}, \qquad (26)$$

where $I_0=I(0)$. For weak two-photon absorption $(I_0\gamma z \ll 1)$, this solution gets reduced to

$$I(z) = I_0(1-I_0\gamma z). \qquad (27)$$

In our experiments, we have the condition (8) and $\gamma\approx 10^{-4}$ cm/MW (see Sec. VI G). Thus, $(I_L\gamma L)\approx 0.15$ and Eq. (27) can be used.

The weak linear absorption with coefficient α is described by the equation

$$I(z) = I_0(1-\alpha z). \qquad (28)$$

It follows from Eqs. (27) and (28) that in our experiments $(I_L\gamma)$ plays the role of α. We can define the total absorption coefficient as

$$\alpha_\Sigma = \alpha + (I_L\gamma), \qquad (29)$$

where $(I_L\gamma)$ is the two-photon contribution. The equivalence should be understood in a quantitative sense. The linear (single-photon) and the two-photon absorption can be treated as similar processes only with respect to the final result of the resonant light-matter interaction, i.e., the irreversible dissipation of electromagnetic into thermal energy. Linear and two-photon absorption are different in terms of quantum mechanical schemes and expressions for the absorption cross section. The physical mechanisms of linear STS-2 and two-photon STS-2 are essentially different, being roughly similar with respect to transformation of temperature fluctuations into permittivity ones.

Why is I_0 replaced by I_L in Eqs. (27)–(29)?

Due to the complexity of the theoretical task, including several connected linear and nonlinear effects, we made the approximation that our pump intensity does not change along the nonlinear interaction length. In accordance with this approximation, we replaced the input intensity I_0 with the pump intensity I_L in Eqs. (27)–(29). This approximation is based on the following considerations. The amplified beam parameters provided conditions for SS very close to its threshold, so that strong pump saturation does not take place. As follows from the title of this paper, there are two main objectives of this study: first, to obtain a pure two-photon STS-2 spectral line, and second, to obtain a pure SBS spectral line. The two-photon STS-2 mechanism should dominate for focusing as hard as possible with linear absorption as weak as possible, i.e., for $F=11$ cm and $\alpha_{\mathrm{MIN}}=0.01$ cm^{-1}. The caustic length is $L_{\mathrm{MIN}}=0.06$ cm. Even for $\alpha_{\mathrm{MAX}}=0.17$ cm^{-1}, $\alpha_{\mathrm{MAX}}L_{\mathrm{MIN}}=0.01$, and $\exp(-0.01)=0.99$. The linear absorption is negligible. The SBS mechanism should dominate for as soft as possible focusing with as weak as possible linear absorption, i.e., for $F=100$ cm and $\alpha_{\min}=0.01$ cm^{-1}. The caustic length is $L_{\max}=6$ cm, $\alpha_{\min}L_{\max}=0.06$, and $\exp(-0.06)=0.94$. The linear absorption is also negligible.

The observation of linear STS-2 in the previous study [22] is not clear (see Sec. III C). Therefore, linear STS-2 also

TABLE V. The two-photon contribution $(I_L\gamma)$ to the total absorption coefficient (29) of hexane at $\lambda=308$ nm for pump intensities I_L corresponding to the three focal lengths F of lens 9 used in our experiments.

F (cm)	I_L (W/cm^2)	$(I_L\gamma)$ (cm^{-1})
11	$\geq 10^{10}$	≥ 1.0
50	10^9	≈ 0.1 (experiment)
100	2.5×10^8	≈ 0.025

calls for further investigation. For $\alpha_{\mathrm{STS}}^{\mathrm{thr}}\approx 0.1$ cm^{-1}, $\alpha_{\mathrm{STS}}^{\mathrm{thr}}L_{\max}=0.6$ and $\exp(-0.6)=0.55$. The linear absorption becomes considerable only for $F=100$ cm (i.e., $L=L_{\max}$) and $\alpha\geq\alpha_{\mathrm{STS}}^{\mathrm{thr}}\approx 0.1$ cm^{-1}.

Under our experimental conditions, the two-photon absorption is constant and equal to $(I_L\gamma L)\approx 0.15$ (see Sec. VI F), and $\exp(-0.15)=0.86$. The two-photon absorption is weak.

G. Calculation of two-photon absorption cross section from the threshold pump intensity for two-photon STS-2

When $(I_L L)=$const, linear STS-2 occurs if $\alpha\geq\alpha_{\mathrm{STS}}^{\mathrm{thr}}$. The two-photon STS-2 must also exhibit threshold behavior, but with respect to $(I_L\gamma)$ rather than α. When the material properties α and γ are kept constant, an increase in I_L caused by a decrease in F leads to different consequences for the total gain $(I_L G_T L)$. It remains invariant for linear STS-2 and increases for two-photon STS-2, because $G_T\propto\alpha=$const [see Eq. (14)] in the former case and $G_T\propto(I_L\gamma)\propto I_L$ in the latter.

The linear and two-photon STS-2 can be distinguished experimentally. If the medium with α and γ such that $\alpha,(I_L\gamma)\ll\alpha_{\mathrm{STS}}^{\mathrm{thr}}$ is used and I_L is gradually increased while $(I_L L)$ is kept constant, the pure two-photon STS-2 component must appear in the spectrum when $(I_L\gamma)\approx\alpha_{\mathrm{STS}}^{\mathrm{thr}}$. Let us find $(I_L\gamma)$. The total gain for STS-2 caused both by the linear and the two-photon absorption (29) reaches the threshold (2) when $\alpha_{\Sigma}^{\mathrm{thr}}\approx\alpha_{\mathrm{STS}}^{\mathrm{thr}}\approx 0.1$ cm^{-1} (Table IV). For $\alpha=0.01$ cm^{-1}, an unshifted component appears in the backscattering spectrum when $I_L^{\mathrm{thr}}\approx 10^9$ W/cm^2 ($F=50$ cm) [Fig. 2(b)]. When $I_L\approx 2.5\times 10^8$ W/cm^2 ($F=100$ cm) there is no unshifted component [Fig. 2(c)], i.e., the threshold is not reached. Since $\alpha=0.01$ cm$^{-1}\ll\alpha_{\mathrm{STS}}^{\mathrm{thr}}\approx 0.1$ cm^{-1}, the unshifted component must be attributed to the pure two-photon STS-2 mechanism. The threshold pump intensity $I_L^{\mathrm{thr}}\approx 10^9$ W/cm^2 can be used to obtain the estimate

$$\alpha_{\Sigma}^{\mathrm{thr}}=\alpha+(I_L^{\mathrm{thr}}\gamma)\approx(I_L^{\mathrm{thr}}\gamma)\approx\alpha_{\mathrm{STS}}^{\mathrm{thr}}\approx 0.1\ \mathrm{cm}^{-1}. \quad (30)$$

For a particular pump wavelength (for $\lambda=308$ nm in our case) the coefficient γ describes a property of the medium (of the chromatography-grade hexane in our case). If $(I_L\gamma)$ is known for one value of I_L (for I_L^{thr} in our case), then it can readily be calculated for other values of I_L. The first column of Table V gives the three focal lengths F of lens 9 used in our experiments; the second column, the three corresponding pump intensities I_L; and the last column, the two-photon contribution $(I_L\gamma)$ to the total absorption coefficient (29).

From $(I_L^{\mathrm{thr}}\gamma)\approx 0.1$ cm^{-1} and $I_L^{\mathrm{thr}}\approx 10^9$ W/cm^2, we can calculate the two-photon absorption coefficient γ and the cross section σ_2. Indeed,

$$\gamma=\frac{I_L^{\mathrm{thr}}\gamma}{I_L^{\mathrm{thr}}}\approx\frac{0.1\ \mathrm{cm}^{-1}}{10^9\ \mathrm{W/cm}^2}\approx 10^{-10}\ \mathrm{cm/W}\approx 10^{-4}\ \mathrm{cm/MW}, \quad (31)$$

$$(I_L\gamma)=\sigma_2 N\frac{I_L}{\hbar\omega}, \quad (32)$$

where $I_L/\hbar\omega$ is the pump intensity in units of photons cm^{-2} s^{-1} and $N=\rho/M$ is the molecular density (M is the molecular mass). For hexane (C_6H_{14}) $N\approx 4\times 10^{21}$ cm^{-3}. The photon energy corresponding to $\lambda=308$ nm is $\hbar\omega\approx 4$ eV$\approx 6.4\times 10^{-19}$ J. We have

$$\sigma_2=\frac{\hbar\omega(I_L^{\mathrm{thr}}\gamma)}{I_L^{\mathrm{thr}}\ N}\approx(2\pm 1)\times 10^{-50}\ \mathrm{cm}^4\ \mathrm{s}. \quad (33)$$

The accuracy is estimated as

$$\frac{\delta\sigma_2}{\sigma_2}\approx\frac{\delta\alpha^{\mathrm{thr}}}{\alpha^{\mathrm{thr}}}+\frac{\delta I_L}{I_L}\approx 0.2+0.3\approx 0.5, \quad (34)$$

where α^{thr} is the experimental threshold value for the linear STS-2.

For comparison, consider the two-photon nonresonant ionization of a many-electron atom at a moderate electric field strength, which does not involve near-threshold absorption, multiple ionization, and perturbation of the atomic spectra. A typical cross section of this process is $\sigma_2^j\approx 10^{-49}-10^{-48}$ cm^4 s [29,30]. Normally, σ_2^j is smaller than the cross section for the two-photon bound-bound transition at the absorption-line center. The value (33) extracted from the experimental data is smaller than σ_2^j. This substantiates our assumption that the main contribution to the STS-2 gain is made by the two-photon absorption. The relatively small value of σ_2 may be explained by the fact that the two-photon absorption scheme ($\lambda/2=154$ nm, hexane) corresponds to a wing of the absorption line.

H. Phase mismatch for SBS caused by two-photon heating

The relationship between $I_L,(I_L\gamma)$ and F (see Table V) explains why the SBS component is not observed for $\alpha=0.01$ cm^{-1} when $F=11$ cm [Fig. 2(a)]. Indeed, in this case $I_L\geq 10^{10}$ W/cm^2, and the total absorption coefficient $\alpha_{\Sigma}=\alpha+(I_L\gamma)\approx(I_L\gamma)\geq 1.0$ cm^{-1} is much larger than the critical value $\alpha_{\mathrm{CR}}\approx 0.1$ cm^{-1} corresponding to phase mismatch (Fig. 4). The heating due to the two-photon absorption is sufficiently strong to cause SBS breakdown.

I. Phase self-modulation and the decrease in phase-conjugation fidelity caused by two-photon heating

We consider only the case of Fig. 3 ($\alpha=0.01$ cm^{-1} =const), when linear absorption (Table V) and linear STS-2 (Table IV) do not contribute. The case of heating due to linear absorption was discussed in [11,12].

TABLE VI. Physical mechanisms of the stimulated backscattering of XeCl ($\lambda=308$ nm) laser pulses with duration $\tau_0\approx 8$ ns in hexane characterized by two typical values of the linear absorption coefficient α, for pump intensities I_L corresponding to the three focal lengths F of lens 9, and $(I_L L)\approx 1.5\times 10^3$ MW/cm (L is the nonlinear interaction length).

		Physical mechanisms of stimulated backscattering	
F (cm)	I_L (W/cm^2)	$\alpha=0.01-0.08$ cm^{-1}	$\alpha=0.17$ cm^{-1}
100	2.5×10^8	SBS	linear STS-2
50	10^9	SBS + two-photon STS-2	linear STS-2 + two-photon STS-2
11	$\geq 10^{10}$	two-photon STS-2	

Assuming that the two-photon absorption plays the dominant role, we replace α with $(I_L\gamma)$ in Eqs. (22)–(24), and the nonlinear phase increment over distance L becomes

$$\delta\Phi(R,t,F)=\delta k,\quad L=\frac{\omega}{c}\left(\frac{\partial n}{\partial T}\right)\frac{\gamma}{\rho c_P}\int_0^t I_L^2(R,\tau,F)L(F)d\tau. \tag{35}$$

The quantity $(I_L^2 L)=I_L(I_L L)$ in Eq. (35) increases with I_L as $(I_L L)=$const, i.e., $\delta\Phi(R,t,F)$ depends on F. The two-photon heating explains the increase in the phase self-modulation of the pump wave when F is reduced from 100 to 11 cm.

The hypersonic grating decay time $\tau_B\approx 1$ ns (see Sec. VI C 3) is shorter than the pump duration by a factor of 8. The phase hologram adjusts to the dynamic variations of the pump field caused by the phase self-modulation due to the two-photon heating. The SBS ensures a high PC fidelity.

The thermal grating decay time $\tau_T\approx 3$ ns (see Sec. VI C 3) is shorter than the pump duration by a factor of 3. The phase hologram cannot keep pace with the dynamic variations of the pump field caused by the phase self-modulation due to two-photon heating. Since the pump wave is scattered by a retarded hologram, the PC fidelity for two-photon STS-2 loses quality.

J. Stimulated scattering mechanisms consistent with the present studies

Table VI summarizes our experimental and theoretical studies of stimulated backscattering of XeCl ($\lambda=308$ nm) laser pulses with the duration $\tau_0\approx 8$ ns in liquid hexane. The first two columns show the three focal lengths F of lens 9 used in our experiments and the corresponding pump intensities I_L. The last two columns list the revealed physical mechanisms of the stimulated backscattering in hexane characterized by two typical values of the linear absorption coefficient $\alpha=0.01-0.08$ cm^{-1} and $\alpha=0.17$ cm^{-1}. Since the nonlinear region is the focal caustic of length L, the quantity $(I_L L)\approx 1.5\times 10^3$ MW/cm remains unchanged for our experiments.

An analysis of the case $I_L\approx 2.5\times 10^8$ W/cm^2 ($F=100$ cm) where the two-photon absorption is insignificant (see Table V), leads to the following conclusions. (1) The presence of linear STS-2 for $\alpha=0.17$ cm^{-1} and its absence for $\alpha=0.01-0.08$ cm^{-1} agree with the estimated threshold value $\alpha_{\mathrm{STS}}^{\mathrm{thr}}\approx 0.1$ cm^{-1} (see Table IV). (2) The absence of SBS for $\alpha=0.17$ cm^{-1} and its presence for $\alpha=0.01-0.08$ cm^{-1} are consistent with the theoretical critical value for the phase mismatch $\alpha_{\mathrm{cr}}\approx 0.1$ cm^{-1} (see Fig. 4). (3) The absence of the SBS + linear STS-2 combination is explained by the fact that $\alpha_{\mathrm{STS}}^{\mathrm{thr}}\approx 0.1$ cm^{-1} is close to $\alpha_{\mathrm{cr}}\approx 0.1$ cm^{-1}, while the step of the variation of α from 0.08 to 0.17 cm^{-1} in our experiments is not sufficiently small to observe both these mechanisms simultaneously. The presence of the SBS + two-photon STS-2 combination indicates that the step of the variation of $\alpha_\Sigma=\alpha+(I_L\gamma)$ in our experiments is sufficient for a simultaneous observation of both mechanisms.

The presence of the linear STS-2 + two-photon STS-2 combination is yet to be substantiated. These two mechanisms are virtually impossible to separate in our experimental spectra. Our theoretical analysis shows that neither linear STS-2 nor two-photon STS-2 can be singled out as the dominant mechanism when $\alpha\geq 0.1$ cm^{-1} and $I_L\geq 10^9$ W/cm^2.

K. Experimental observation of a genuine SBS line in the near-ultraviolet region

According to the existing theory, which takes into account linear absorption (see Table IV and Fig. 4), only SBS can play a role in our experiments when $\alpha<0.1$ cm^{-1}, while only linear STS-2 can contribute when $\alpha>0.1$ cm^{-1} (in view of phase mismatch for SBS). It is not surprising that these two mechanisms are listed in the last column of Table I as those suggested in the previous studies. Both SBS and linear STS-2 in Table I are incorrect. Indeed, it follows from the third column of Table I that $I_L\geq 10^{10}$ W/cm^2 in all the previous studies. However, according to Table VI, for $I_L\geq 10^{10}$ W/cm^2, either two-photon STS-2 or the linear STS-2 + two-photon STS-2 combination should be observed in hexane when $\alpha<0.1$ cm^{-1} and $\alpha>0.1$ cm^{-1}, respectively. Therefore SBS should be replaced by two-photon STS-2 in all rows of Table I with the exception of the last one, while linear STS-2 should be replaced with the linear STS-2 + two-photon STS-2 combination in the last row. This consideration is corroborated by the fact that the measured frequency shift Ω in the fourth column of Table I is much smaller than the Brillouin shift Ω_B predicted theoretically for the same λ (Table II). It can be concluded that the genuine SBS line has not been observed in previous studies

of the stimulated scattering in the near-uv region.

In our experiments the stimulated scattering of near-uv ($\lambda=308$ nm) laser radiation in hexane was studied, and a SBS line with frequency shift equal to 0.33 cm^{-1} [see Figs. 2(b) and 2(c)], in full agreement with the theory (see Table II), was observed. To observe the genuine SBS line, we had to reduce the pump intensity from $I_L \geq 10^{10}$ W/cm^2 [Fig. 2(a)] as in previous studies (Table I) to $I_L \leq 10^9$ W/cm^2 [Figs. 2(b) and 2(c)], while keeping the total gain for SBS (Table IV) invariant. This made it possible to reduce the two-photon contribution to the total absorption coefficient (Table V) and to weaken the effect of the SBS phase mismatch due to two-photon heating.

L. Effects of self-focusing and plasma formation on stimulated scattering

All light-producing phenomena were inspected visually through a thin transparent glass wall of the cell. First, consider self-focusing. There are two mechanisms responsible for self-focusing—the Kerr effect and electrostriction [31]. The relaxation time for the Kerr effect is $\tau_K \approx 10^{-11}$ s. The relaxation time for electrostriction is approximately equal to the time for the acoustic wave to pass through the focal caustic diameter. The minimal value for this time under our experimental conditions is

$$\tau_{\mathrm{STR}}^{\min} \approx \frac{F_{\min}\theta}{v} \approx \frac{(11\ \mathrm{cm})(3\times 10^{-4}\ \mathrm{rad})}{10^5\ \mathrm{cm/s}} \approx 3\times 10^{-8}\ \mathrm{s} = 30\ \mathrm{ns},$$

which is considerably more than the pump pulse duration $\tau_0 \approx 8$ ns. Therefore, as well as in [32,33], under our experimental conditions only the Kerr effect should be taken into account. The self-focusing is characterized by the critical power [34]

$$P_{\mathrm{cr}} = \frac{(1.22\lambda)^2 4\pi c}{128 c n n_2} = \frac{\pi(1.22\lambda)^2}{32 n n_2} \approx 8\times 10^5\ \mathrm{W},$$

where $n_2 \approx 4\times 10^{-13}$ ESU $\approx 1.2\times 10^{-12}$ cm^2/kW is the Kerr constant of hexane [26]. Our pump power is

$$W_L \approx \frac{1.5\ \mathrm{mJ}}{8\ \mathrm{ns}} \approx 2\times 10^5\ \mathrm{W} \approx 0.25\ P_{\mathrm{cr}}.$$

For the input power $P < 0.273 P_{\mathrm{cr}}$ self-focusing does not develop [34]. Hence, self-focusing should not affect our experiments. Usually, self-focusing in liquids is followed by thin channels of light [35] and by increase in the divergence angle of the radiation passing through the cell in the forward direction. A visual inspection of the nonlinear liquid and the radiation did not show these signs of self-focusing.

Second, consider plasma formation. The acoustic wave generated as a result of SBS is supposed to be the reason for optical destruction in solids [7,36]. The dynamics of internal optical destruction in solids was studied in [37]. During the course of the laser pulse, the destruction has the form of a thread placed along the focal caustic. The pace of thread development is much higher than the speed of a shock wave. The thread diameter is considerably smaller than the focal caustic diameter. Subsequent to the laser pulse the destruction grows in the transverse direction and possesses the form of disks. The SBS cannot completely provide the energy transformation. Preference is given to the destruction mechanisms associated with self-focusing and multiphoton ionization.

A theory of the optical breakdown in liquids does not exist, because not much is known about it [1,34]. For $\hbar\omega = 4$ eV fast three-photon ionization of hexane provides the initial electrons. The breakdown threshold depends on the electron multiplication rate. Different approaches (classical or quantum) are used to describe how the electron gains energy, depending on the relation between the photon energy $\hbar\omega$ and the average electron energy increment during a single collision, $\Delta\varepsilon$ [38]. If $\Delta\varepsilon \gg \hbar\omega$, the classical kinetic equation can be used. If $\hbar\omega \geq \Delta\varepsilon$, the quantum kinetic equation containing finite-difference expressions should be used. For our moderate pump intensity $I_L < 10^{11}$ W/cm^2, we have $\Delta\varepsilon \approx 1$ eV. Since $\hbar\omega = 4$ eV $> \Delta\varepsilon \approx 1$ eV, the quantum kinetic equation should be solved.

As a rough approximation, a liquid could be considered as a gas under ultrahigh pressure of thousands of atmospheres. For the noble gases under thousands of atmospheres [38,39] the optical breakdown threshold reaches $E \approx 10^6$ V/cm, $I \approx (E/20)^2 \approx 2.5\times 10^9$ W/cm^2. For molecular gases [38,40] the thresholds are hundredfolds higher than for single-atom gases, because it is more difficult for the electron to pass the "dangerous" region between excitation and ionization.

Usually, the optical breakdown in a liquid is followed by a flash of light [35] and bubbles. That was not detected by visual inspection. It is possible that for organic liquids like hexane the electromagnetic energy is transmitted to hydrodynamic perturbations instead of an avalanche. The emergence of SBS and STS-2 in our experiments confirms this supposition.

VII. SUMMARY

The present study focuses on the stimulated scattering of nanosecond (5–10 ns) near-uv ($\lambda = 193-351$ nm) laser pulses in liquids (hexane, heptane, and others). Some experimental results gained from previous studies concerning the frequency shift and phase-conjugation fidelity disagree with the existing theory of SS, which was developed for the near-ir ($\lambda = 0.69-1.06$ μm) spectral region and takes into account only linear (single-photon) light absorption.

To resolve the inconsistency, SS of XeCl excimer laser radiation ($\lambda = 308$ nm) with the duration 8 ns in liquid hexane for various values of the linear absorption coefficient α and the pump intensity I_L was investigated experimentally. In contrast to the previous near-uv studies, we managed to create a master oscillator, running in a single longitudinal mode. As is well known, this mode of operation is characterized not only by a small spectrum, but also by a near-Gaussian temporal behavior without uncontrolled intensity peaks (mode interference). So our estimates of the pump intensity were much more reliable than previous ones. Due to the smaller bandwidth, we had less amplified beam energy and limited

experimental possibilities as compared to the previous studies (we could not use neutral filters to control the pump intensity). We also managed to create a spectrum analyzer, which monitored the temporal spectra of two counterpropagating pulses in different but close enough fields. It allowed us to be sure that the right field involves only a pump spectrum, and the left field only a backscattered spectrum. Without such an analyzer, any slightly shifted backscattered spectral line may be simply confused with the spectral line of the pump radiation.

When the product $(I_L L) \approx 1.5 \times 10^3$ MW/cm (L is the nonlinear interaction length) remains invariant, the experimental SS spectrum depends not only on α, but also on I_L. For $\alpha < 0.1$ cm^{-1} and $I_L \geq 10^{10}$ W/cm^2, the spectrum includes a line corresponding to the mechanism of stimulated thermal scattering induced by the heating due to two-photon absorption. For $\alpha < 0.1$ cm^{-1} and $I_L \leq 10^9$ W/cm^2, the spectrum includes a line in the near-uv region, which corresponds to genuine stimulated Brillouin scattering and is characterized by the frequency shift $\Omega_B = 0.33$ cm^{-1}, in full agreement with the theory. For $\alpha > 0.1$ cm^{-1} or $I_L \geq 10^{10}$ W/cm^2, SBS is suppressed by phase mismatch due to heating caused by the linear or two-photon absorption, respectively. To detect the genuine SBS line for $\alpha < 0.1$ cm^{-1}, we had to reduce the pump intensity while keeping constant the total gain for SBS, and thus weaken the phase mismatch due to the two-photon heating.

When two-photon STS-2 is used for phase conjugation, the PC fidelity is lower than that achieved by using SBS because of the two-photon thermal phase self-modulation. The molecular cross section for the two-photon absorption of hexane at $\lambda = 308$ nm, $\sigma_2 \approx (2 \pm 1) \times 10^{-50}$ cm^4 s, is found from the experimental threshold pump intensity for two-photon STS-2.

The SBS lines observed in previous studies have frequency shifts much smaller than those predicted by the theory and must be interpreted as two-photon STS-2 lines. The physical mechanisms of linear STS-2 and two-photon STS-2 are essentially different and their lines can readily be distinguished in the spectrum. The total inconsistency between the experimental behavior of two-photon and linear STS-2 lines explains why the two-photon STS-2 lines observed in the previous studies were attributed to SBS for almost a decade. The physical mechanism of two-photon STS-2 is not specific for the near-uv spectral region.

[1] Y. R. Shen, *The Principles of Nonlinear Optics* (Wiley-Interscience, New York, 1984/Nauka, Moscow, 1989/Wiley-Interscience, Hoboken, NJ, 2003).

[2] S. Kielich, *Molecular Nonlinear Optics* (PWN, Warsaw, 1977/Nauka, Moscow, 1981); J. R. Lalanne, A. Ducasse, and S. Kielich, *Laser-Molecule Interaction: Laser Physics and Molecular Nonlinear Optics* (Wiley, New York, 1996).

[3] V. G. Dmitriev, *Nonlinear Optics and Phase Conjugation* (Fizmatlit, Moscow, 2003) (in Russian).

[4] B. Ya. Zeldovich, N. F. Pilipetsky, and V. V. Shkunov, *Principles of Phase Conjugation* (Nauka, Moscow, 1985/Springer-Verlag, Berlin, 1985).

[5] I. L. Fabelinskii, *Molecular Scattering of Light* (Nauka, Moscow, 1965/Plenum, New York, 1968).

[6] B.Ya. Zeldovich, V.I. Popovichev, V.V. Ragulskii, and F.S. Faizullov, Zh. Eksp. Teor. Fiz. Pis'ma Red. **15**, 160 (1972) [JETP Lett. **15**, 109 (1972)].

[7] R. Y. Chiao, C. H. Townes, and B. P. Stoicheff, Phys. Rev. Lett. **12**, 592 (1964).

[8] E. Garmire and C. H. Townes, Appl. Phys. Lett. **5**, 84 (1964).

[9] R. G. Brewer and K. E. Rieckhoff, Phys. Rev. Lett. **13**, 334 (1964).

[10] R. G. Brewer, Appl. Phys. Lett. **5**, 127 (1964).

[11] V. V. Kuzmin, Tr. Fiz. Inst. P. N. Lebedeva, Akad. Nauk SSSR **207**, 3 (1991); *Non-Linear Optics and Molecular Light Scattering*, edited by N. G. Basov and I. L. Fabelinskii (Nauka, Moscow, 1991) (in Russian).

[12] S. F. Grigoriev, O. P. Zaskalko, and V. V. Kuzmin, Zh. Eksp. Teor. Fiz. **92**, 1246 (1987) [Sov. Phys. JETP **65**, 697 (1987)].

[13] V. S. Starunov, Zh. Eksp. Teor. Fiz. **57**, 1012 (1969) [Sov. Phys. JETP **30**, 553 (1970)].

[14] V. S. Starunov and I. L. Fabelinskii, Usp. Fiz. Nauk **98**, 441 (1969) [Sov. Phys. Usp. **12**, 463 (1970)]..

[15] M. Statkine, I. J. Bijio, B. J. Feldman, and R. A. Fisher, Opt. Lett. **7**, 108 (1982).

[16] M. C. Gower, Opt. Lett. **7**, 423 (1982).

[17] M. C. Gower, Opt. Lett. **8**, 70 (1983).

[18] E. Armandillo and D. Proch, Opt. Lett. **8**, 523 (1983).

[19] M. C. Gower and R. G. Caro, Opt. Lett. **7**, 162 (1982).

[20] G. M. Davis and M. C. Gower, IEEE J. Quantum Electron. **27**, 496 (1991).

[21] S. S. Alimpiev, V. S. Bukreev, S. K. Vartapetov, I. A. Veselovskii, V. S. Nersisian, A. Z. Obidin, and A. M. Prokhorov, Kratk. Soobshch. Fiz. **12**, 11 (1989) [Sov. Phys. Lebedev. Inst. Rep. **12**, 12 (1989)].

[22] S. S. Alimpiev, V. S. Bukreev, S. K. Vartapetov, I. A. Veselovskii, B. I. Kusakin, S. V. Lihanckii, and A. Z. Obidin, Kvantovaya Elektron. (Moscow) **18**, 89 (1991) [Sov. J. Quantum Electron. **21**, 80 (1991)].

[23] A. L. Egorov, V. V. Korobkin, and R. V. Serov, Kvantovaya Elektron. (Moscow) **2**, 513 (1975) [Sov. J. Quantum Electron. **5**, 291 (1975)].

[24] A. J. Alcock, C. De Michelis, and M. C. Richardson, IEEE J. Quantum Electron. **6**, 622 (1970).

[25] V. F. Nozdrev, *The Use of Ultrasonics in Molecular Physics* (Fizmathlit, Moscow, 1958/Pergamon Press, Oxford, 1965).

[26] P. P. Ho and R. R. Alfano, Phys. Rev. A **20**, 2170 (1979).

[27] A. J. Gordon and R. A. Ford, *The Chemist's Companion* (Wiley, New York, 1972).

[28] Yu. N. Karamzin, A. P. Sukhorukov, and V. A. Trofimov, *Mathematical Modeling in Nonlinear Optics* (Moscow State University Press, Moscow, 1989) (in Russian).

[29] M. Ammosov, N. Delone, M. Ivanov, I. Bondar, and A. Masalov, Adv. At., Mol., Opt. Phys. **29**, 34 (1992).

[30] N. B. Delone and V. P. Krainov, *Fundamentals of Nonlinear Optics of Atomic Gases* (Nauka, Moscow, 1986/Wiley, New York, 1988).
[31] R. Y. Chiao, E. Garmire, and C. H. Townes, Phys. Rev. Lett. **13**, 479 (1964).
[32] Y. R. Shen, Phys. Lett. **20**, 378 (1966).
[33] P. Lallemand and N. Blombergen, Phys. Rev. Lett. **15**, 1010 (1965).
[34] J. F. Reintjes, *Nonlinear Optical Parametric Processes in Liquids and Gases* (Academic Press, New York, 1984/Mir, Moscow, 1987).
[35] R. G. Brewer and J. R. Lifsits, Phys. Lett. **23**, 79 (1966).
[36] C. R. Giuliano, Appl. Phys. Lett. **5**, 137 (1964).
[37] J. P. Budin and J. Raffy, Appl. Phys. Lett. **9**, 291 (1966).
[38] Yu. P. Raizer, *Laser-Induced Discharge Phenomena* (Nauka, Moscow, 1974/Consultants Bureau, New York, 1977).
[39] D. H. Gili and A. A. Dougal, Phys. Rev. Lett. **15**, 845 (1965).
[40] Yu. B. Afanasiev, Ye. M. Belenov, and I. A. Poluektov, Zh. Eksp. Teor. Fiz. Pis'ma Red. **15**, 60 (1972) [JETP Lett. **15**, 41 (1972)].